Differences between surface and column atmospheric CO_2 and implications for carbon cycle research

Seth C. Olsen[1] and James T. Randerson[1,2,3]

Received 9 July 2003; revised 13 October 2003; accepted 29 October 2003; published 16 January 2004.

[1] We used a three-dimensional atmospheric transport model to investigate several aspects of column CO_2 that are important for the design of new satellite-based observation systems and for the interpretation of observations collected by Sun-viewing spectrometers. These aspects included the amplitude of the diurnal cycle and how it is related to surface fluxes, the amplitude and phase of the seasonal cycle, and the magnitude of the north-south hemispheric gradient. In our simulation, we found that column CO_2 had less variability than surface CO_2 on all scales. The annual mean column CO_2 north-south gradient and seasonal cycle amplitude were approximately one half of their surface counterparts and the column CO_2 diurnal amplitude rarely exceeded 1 ppm. A 1 Gt C yr^{-1} Northern Hemisphere carbon sink decreased the north-south column CO_2 gradient by $\sim$0.4 ppm. *INDEX TERMS:* 0315 Atmospheric Composition and Structure: Biosphere/atmosphere interactions; 0368 Atmospheric Composition and Structure: Troposphere—constituent transport and chemistry; 1610 Global Change: Atmosphere (0315, 0325); 1615 Global Change: Biogeochemical processes (4805); *KEYWORDS:* column CO_2, CO_2 sources and sinks, biosphere-atmosphere exchange, atmospheric transport, diurnal cycle

Citation: Olsen, S. C., and J. T. Randerson (2004), Differences between surface and column atmospheric CO_2 and implications for carbon cycle research, *J. Geophys. Res.*, *109*, D02301, doi:10.1029/2003JD003968.

1. Introduction

[2] While diurnal, seasonal, and latitudinal aspects of CO_2 variability have been extensively explored near the surface [e.g., *Bolin and Keeling*, 1963; *Keeling et al.*, 1976; *Fung et al.*, 1987; *Wofsy et al.*, 1988; *Tans et al.*, 1990; *Bakwin et al.*, 1995; *Denning et al.*, 1996a; *Chou et al.*, 2002; *Gurney et al.*, 2002] much less is known about the behavior of the CO_2 column integral. Column CO_2 measurements are likely to become abundant and largely independent constraints on carbon cycle processes, both from the deployment of ground-based Fourier transform infrared spectrometers that use the Sun as a light source [e.g., *Wallace and Livingston*, 1990; *Yang et al.*, 2002], and from future space-based spectrometers, such as NASA's Orbiting Carbon Observatory (OCO). Several recent modeling studies have explored how column CO_2 observations would help to reduce uncertainties associated with carbon sources and sinks in atmospheric inversions. *Rayner and O'Brien* [2001] demonstrated that at a coarse resolution ($8^\circ \times 10^\circ$), monthly mean column CO_2 observations with a precision of 2.5 ppm or less would exceed the capability of existing surface observation networks in identifying continental-scale distributions of sources and sinks. This result was found to be robust using simulated satellite observations that included realistic satellite orbit, scan geometry, and cloud cover characteristics [*Rayner et al.*, 2002]. In this same study, however, source/sink inversion results were found to be sensitive to biases caused by incomplete sampling of the diurnal cycle of column CO_2.

[3] The reduced uncertainty associated with the use of column CO_2 in atmospheric inversions, arises, in part, from greater sampling of CO_2 in the tropics where relatively strong vertical convection and relatively weak horizontal winds limits the effectiveness of existing surface observations. For example, *Gloor et al.* [2000] showed that measurements of a single column profile of CO_2 over the Amazon Basin would be one of the most effective ways, paradoxically, to reduce uncertainty associated with the size of the contemporary north American carbon sink. Other types of free-troposphere CO_2 observations that sample the remote tropical troposphere may have comparable advantages. Specifically, *Pak and Prather* [2001] provided evidence that horizontal profiles of CO_2 in the free troposphere from a limb sounding spectrometer would yield improvements in source/sink characterizations of similar magnitude to that predicted for column observations.

[4] While these initial studies have explored the applicability of column measurements to the CO_2 source/sink problem, there are other dimensions of column CO_2 that remain relatively unexplored and potentially affect the design of new satellite and ground based column CO_2 observation systems and the interpretation of column data for the study of continental-scale biological processes. Here we compare the diurnal, seasonal, and latitudinal variability

[1]Division of Geological and Planetary Sciences, California Institute of Technology, Pasadena, California, USA.
[2]Also at Division of Engineering and Applied Science, California Institute of Technology, Pasadena, California, USA.
[3]Now at Department of Earth System Science, University of California at Irvine, Irvine, California, USA.

0148-0227/04/2003JD003968

of column CO_2 with that at the surface, using column, flask, aircraft, and continuous CO_2 observations as a check on model behavior at multiple scales. We specifically address the questions of 1) what is the amplitude of diurnal variation of column CO_2 and how does it relate to surface fluxes, 2) how does the amplitude and phase of the column CO_2 seasonal cycle compare with surface observations, and 3) what is the magnitude of the north-south interhemispheric gradient?

2. Methods

2.1. Model Description

[5] We simulated the distribution of atmospheric CO_2 with the Model of Atmospheric Transport and Chemistry (MATCH) three-dimensional atmospheric transport model. MATCH represents advective transport using a combination of horizontal and vertical winds and has parameterizations of wet and dry convection and boundary layer turbulent mixing. Versions of MATCH have been used previously in studies of stratospheric transport [*Rasch et al.*, 1994; *Waugh et al.*, 1997], tropospheric aerosols [*Collins et al.*, 2001; *Rasch et al.*, 2001], radon [*Mahowald et al.*, 1997], and atmospheric CO_2 [*Dargaville et al.*, 2002, 2003]. MATCH is an off-line model that uses archived meteorological fields which for this study were derived from the NCAR Community Climate Model version 3 with T21 horizontal resolution (approximately 5.5° latitude × 5.5° longitude) and 26 vertical levels from the surface up to 0.2 hPa (about 60 km) on hybrid sigma pressure levels. These meteorological fields do not represent any specific year but a climatologically "average" year. The top of the first model level is approximately 110 m. This meteorological data was archived every 3 model hours and was interpolated to the 30-min time step used in MATCH. In this configuration MATCH has an interhemispheric transport time of approximately 0.74 years, about in the middle of the 0.55 year to 1.05 year range of the models that participated in the TransCom 2 experiment [*Denning et al.*, 1999a]. A single year of dynamical inputs was recycled for the multiyear runs used in this study.

2.2. Surface Fluxes

[6] We considered three separate types of CO_2 surface fluxes: (1) emissions from fossil fuel use, cement manufacturing, and gas flaring, (2) gas exchange with the oceans, and (3) terrestrial biosphere net ecosystem production (NEP). The emissions from fossil fuel, hydraulic cement manufacturing, and gas-flaring (5.8 Gt C yr^{-1}) were based on a 1° × 1° map for the year 1990 [*Andres et al.*, 1996]. These fluxes were uniformly distributed throughout the year. The ocean sink (−2.2 Gt C yr^{-1}) was adapted from 1° × 1° monthly mean CO_2 fluxes derived from sea-surface pCO_2 measurements [*Takahashi et al.*, 1999]. These monthly fluxes were linearly interpolated between the monthly values. A diurnally varying NEP flux was constructed from two one-way flux components: gross primary production (GPP) and ecosystem respiration (R_e). At each grid box we estimated monthly GPP as two times the net primary production (NPP) from the Carnegie-Ames-Stanford Approach (CASA) biosphere model [*Randerson et al.*, 1997]. Within each month GPP was distributed according to a downward shortwave radiation flux from the National Center for Environmental Prediction (NCEP) data assimilation model for the year 2000. From the six hour resolution NCEP flux data we estimated the flux at three hour intervals by fitting the NCEP data to a theoretical clear-sky solar radiation function that depended on time of day, Julian day, latitude, and longitude. Monthly R_e was distributed within each month according to a function depending on temperature, a unitless Q_{10} constant, and a normalization constant, $R_{e,o}$.

$$R_e(t) = R_{e,o} \times Q_{10}^{\left(\frac{T(t)-T_o}{10}\right)}$$

The temperature at each grid box, estimated from NCEP 2 m air temperature for the year 2000, was linearly interpolated to a three hour interval. We used a Q_{10} value of 1.5 and $R_{e,o}$ was subsequently chosen such that the monthly NEP flux (GPP-R_e) was the same as previous CASA estimates used by *Randerson et al.* [1997] and *Gurney et al.* [2002]. The model sources were updated every three hours and the mixing ratio at each model grid point was saved every two hours during the final year of the 6 year model simulation.

[7] We did not include a "missing" carbon sink necessary to balance fossil carbon sources with the current atmospheric CO_2 growth rate [e.g., *Tans et al.*, 1990; *Gurney et al.*, 2002] in our analysis.

2.3. Daytime Net Flux

[8] As part of our analysis we present observations and model estimates of a parameter relevant to the diurnal variation in column CO_2, the daytime net flux (DNF). We define the DNF as the daily accumulation of net ecosystem exchange (NEE) during the daylight period when photosynthesis is greater than ecosystem respiration (with units of gC m^{-2} d^{-1}). The DNF is analogous to the concept of growing season net flux (GSNF) used by *Fung et al.* [1983] and *Knorr and Heimann* [1995] to evaluate the effect of surface fluxes on the seasonal cycle of atmospheric CO_2. In an isolated column (an atmospheric column with no horizontal mixing) the column diurnal amplitude is directly proportional to DNF and can be simply calculated from the DNF for the case of a diurnally varying flux that is in balance (neither a source nor a sink) over a 24 hour period. In our model the magnitude of the DNF was generally large over regions with an active terrestrial biosphere (Table 1).

3. CO_2 Data Sources

3.1. Eddy Covariance Fluxes

[9] To evaluate our relatively simple model of diurnal fluxes, we compared our results with eddy covariance measurements from several regions. At each eddy flux site an average diurnal cycle of CO_2 fluxes was constructed from the eddy covariance measurements over a period of several weeks. The DNF was then calculated from this average cycle. We used data from seven sites in three regions in our analysis, representing peak growing season conditions in the high northern latitudes, middle northern latitudes, and tropics (Table 2).

[10] In high northern latitudes, we used data from two tower sites that were located near Delta Junction Alaska, USA. The two sites were about 10 km apart and occupied

Table 1. Regional Differences in DNF and Surface and Column Diurnal Amplitudes

	January			July		
		Amplitude, ppm			Amplitude, ppm	
Region	DNF, gC m^{-2} d^{-1}	Surface	Column	DNF, gC m^{-2} d^{-1}	Surface	Column
Eurasia, 50°N–90°N	0.00	0.52	0.05	−3.16	17.77	0.58
North America, 50°N–90°N	0.00	0.34	0.04	−2.23	12.71	0.43
Eurasia, 22°N–50°N	−0.13	2.49	0.06	−1.34	8.81	0.30
North America, 22°N–50°N	−0.07	3.09	0.06	−3.05	22.45	0.63
Congo	−2.20	29.07	0.59	−1.84	25.99	0.44
Amazon Basin	−3.37	32.20	0.73	−4.33	33.73	0.89
Africa, south of 0°	−2.62	16.08	0.53	−0.84	10.90	0.22
Australia	−0.49	5.00	0.13	−0.58	3.79	0.12
South America, south of 20°S	−2.96	20.02	0.62	−0.76	11.03	0.19
Pacific Ocean, 50°N–90°N	0.00	0.11	0.04	0.00	0.43	0.10
Southern Ocean, south of 50°S	0.00	0.07	0.01	0.00	0.04	0.02

the same model grid box (64°N, 146°W). One site was located in a relatively homogeneous black spruce (*Picea mariana*) forest that had a mean canopy height of 4.5 m and a stand age of ~80 years. The second site was located in an aspen (*Populus tremuloides*) forest that had a mean canopy height of 5 m and a stand age of 15 years (the site burned in 1987). Eddy covariance measurements have been made at these sites since September 2001 using a CSAT3 sonic anemometer to measure wind velocity and virtual temperature fluctuations and a LiCor 7500 infrared gas analyzer to determine water vapor and CO_2 density fluctuations. Fluxes of sensible and latent heat and CO_2 were calculated from 30 min covariances of 10 Hz data. We compared peak summer DNF (13 June to 12 July 2002) from these sites with the modeled DNF (described above) sampled over the same seasonal period.

[11] In middle northern latitudes, we used data from three sites that were located in the Chequamegon-Nicolet National Forest in northern Wisconsin, USA and were part of the Chequamegon Ecosystem-Atmosphere Study (ChEAS) (http://cheas.psu.edu). All of these sites occupied the same model grid box (46°N, 90°W). The first tower (Park Falls/WLEF) was 447 m high and was surrounded by boreal lowland and wetland forests. The surrounding canopy had approximately 70% deciduous and 30% conifer trees, and a mean canopy height of ~20 m. Hourly CO_2 fluxes were calculated at 30 m, 120 m, and 396 m. Flux measurements at this site are described by *Berger et al.* [2001], and NEE data for 1997 are discussed by *Davis et al.* [2003]. The second tower (Lost Creek) was located in an alder-willow wetland. The mean canopy height was 1–2 m and eddy flux measurements were made at 10 m. The third site (Willow Creek) was located in temperate/boreal lowland and wetland forest. The canopy height was ~24 m and eddy flux measurements were made at 30 m. We used data from 19 July to 17 August 2001 in our comparison with modeled surface fluxes.

[12] In the tropics, we used data from two sites located within the Amazon Basin. The first was located in the Ducke Forest Reserve near Manaus, Brazil (3°S, 60°W). Data at this site were gathered during the wet season as part of the Amazon Boundary Layer Experiment (ABLE-2B) [*Fan et al.*, 1990; *Harriss et al.*, 1990]. Fluxes of CO_2 and O_3 were measured over the period from 22 April to 8 May 1987. *Fan et al.* [1990] report an average daytime (6–18 hours) NEE of about −4.4 KgC ha^{-1} h^{-1} (equivalent to a DNF of −5.28 gC m^{-2} d^{-1}). The forest canopy height was approximately 30 m. The other Amazon site was located at Reserva Jaru, Rondonia, Brazil (10°S, 62°W). Data at this site were gathered as part of the Anglo-Brazilian Amazonian Climate Observation Study (ABRACOS) (http://tucupi.cptec.inpe.br/abracos). The forest was palm-rich with a canopy height of about 30 m. CO_2 flux measurements were made during September 1992 and from April to June 1993 [*Grace et al.*, 1995a, 1995b]. We compared the observed DNF from an average diurnal CO_2

Table 2. Observed and Modeled Daytime Net Flux (DNF)

	Observations		DNF, gC m^{-2} d^{-1}		Modeled Diurnal Amplitude, ppm		
Site	Location	Time Period	Observed	Model[a]	MATCH Surface	MATCH Column	Isolated Column[b]
Alaska, Aspen	64°N, 146°W	12 Jun to 12 Jul 2002	−2.69	−2.49	16.5	0.41	0.58
Alaska, Spruce	64°N, 146°W	12 Jun to 12 Jul 2002	−1.72	−2.49	16.5	0.41	0.58
Wisconsin, Park Falls/WLEF	46°N, 90°W	19 Jul to 17 Aug 2001	−3.14	−4.54	22.8	0.84	1.06
Wisconsin, Lost Creek	46°N, 90°W	19 Jul to 17 Aug 2001	−3.35	−4.54	22.8	0.84	1.06
Wisconsin, Willow Creek	46°N, 90°W	19 Jul to 17 Aug 2001	−6.15	−4.54	22.8	0.84	1.06
Amazon, Rondonia	10°S, 62°W	16 May to 15 Jun 1993	−3.80	−4.70	32.2	0.93	1.10
Amazon, Ducke	3°S, 60°W	22 Apr to 8 May 1987	−5.28	−2.97	28.8	0.62	0.69

[a]Model data were taken from grid box containing tower observation site and during the same seasonal period.

[b]The isolated column estimates of the diurnal amplitude were obtained using the model DNF and assuming that there was no horizontal mixing from adjacent regions and that biospheric fluxes were balanced when integrated over a 24 hour period. With these assumptions, the amplitude of the isolated column at sea level is equal to 0.234 ppm/gC m^{-2} d^{-1} * DNF.

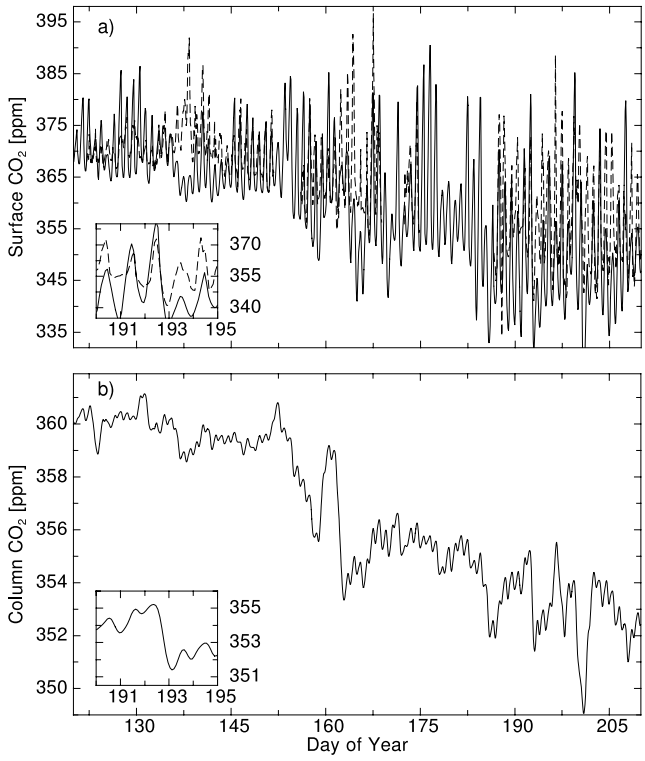

Figure 1. (a) Surface and (b) column CO_2 at the Park Falls/WLEF tower site simulated using the MATCH model and surface fluxes described in the text. Surface observations at a height of 76 m from *Bakwin et al.* [1998] during the period from 30 April (day 120) to 29 July (day 210) 1996 are represented with a dashed line, and MATCH model results from the first model level ($\sim$0–110 m) are represented with a solid line. Insets show a portion of the data on an expanded scale and in Figure 1a allow a comparison of the phase of model and observed diurnal cycles. A single scalar offset was added to the model simulations so that the observed and modeled CO_2 concentrations were equal at the beginning of the period.

flux cycle from 16 May to 15 June 1993 to the modeled average DNF over that same period.

3.2. Flask Observations

[13] We used CO_2 flask observations from the National Oceanic and Atmospheric Administration's (NOAA) Climate Monitoring and Diagnostics Laboratory (CMDL) at selected sites to compare with model simulations on seasonal timescales. Most surface sampling sites in the NOAA network are in remote marine environments, represent well mixed tropospheric air, and provide a good overview of the large-scale features and month to month trends in the global distribution of atmospheric CO_2 [*Conway et al.*, 1994; *Masarie and Tans*, 1995]. In our analysis we focused on three sites: Alert Bay, Canada (82°N, 62°W), Cape Kumukahi, USA (19°N, 204°E), and Cape Grim, Australia (40°S, 144°E). For comparison with model results we constructed a mean seasonal cycle using data from January 1990 to December 1995. We estimated the variability of the monthly mean from the standard deviation of the linearly detrended monthly data. For example, the data from each January were detrended and then the standard deviation of that detrended data was used as an estimate of the variability of the January monthly mean.

3.3. High-Resolution Time Series

[14] Measurements of CO_2 mixing ratio from the Park Falls/WLEF tall tower were used to assess the behavior of model CO_2 concentrations on diurnal and synoptic timescales. Mixing ratio data were reported hourly from 11, 30, 76, 122, 244, and 396 m heights [*Bakwin et al.*, 1998]. We compared results from the first model level (approximately 110 m top) with the 76 m tower data. The tower observations spanned the period from May to July 1996. Changes of CO_2 mixing ratios at WLEF resulting from synoptic-scale processes are discussed by *Hurwitz et al.* [2003].

3.4. Aircraft Observations

[15] We used profiles of atmospheric CO_2 made from aircraft during ABLE-2B (13 April to 5 May 1987) to evaluate the ability of the model to reproduce the vertical structure in diurnal variability of CO_2 in the Amazon basin (3°S, 60°W). CO_2 was measured during 21 aircraft missions including 85 vertical profiles from about 0.15 to 6 km over the hours from 0700 to 1700 local time [*Fan et al.*, 1990; *Chou et al.*, 2002]. Data from flights within the model grid box (flight numbers 7, 8, 9, 13, 14, 15, 16, 18, 19, 20, and 21) were combined and averaged by hour and 200 m altitude bins for comparison with modeled profiles. Each altitude-time bin contained between 2 and 279 observations.

3.5. Column Observations

[16] Recent measurements of column CO_2 from the Kitt Peak observatory in Arizona, USA (32°N, 112°W, elevation 2083 m) were used to compare with the model simulation. *Yang et al.* [2002] retrieved the CO_2 and O_2 column from high-resolution solar absorption spectra obtained from the McMath telescope Fourier transform spectrometer over the period from 1977 to 1995 as a reanalysis of previous work by *Wallace and Livingston* [1990]. On the basis of spectra collected when solar zenith angles were less than 80°, the amplitude of the column seasonal cycle is approximately 5.7 ppm (peak to peak) and its phase is closer to that observed at Mauna Loa than to that observed at Niwot Ridge, even though Kitt Peak is much closer to Niwot Ridge than to Mauna Loa. *Yang et al.* [2002] suggest that this is because both Kitt Peak column and Mauna Loa surface measurements are more representative of free troposphere air while Niwot Ridge data are more heavily influenced by continental CO_2 sources and sinks.

4. Results and Discussion

4.1. Diurnal Column Variability in the Continental Interior of North America

[17] At the Park Falls/WLEF tower site surface observations show that the amplitude of the diurnal cycle increases from May (day 121) through the end of July (day 210) and is superimposed on a downward trend caused by increasing photosynthetic activity in the Northern Hemisphere (Figure 1a). The amplitude of the diurnal cycle is highly variable from day to day and driven largely by synoptic-scale weather variability that simultaneously

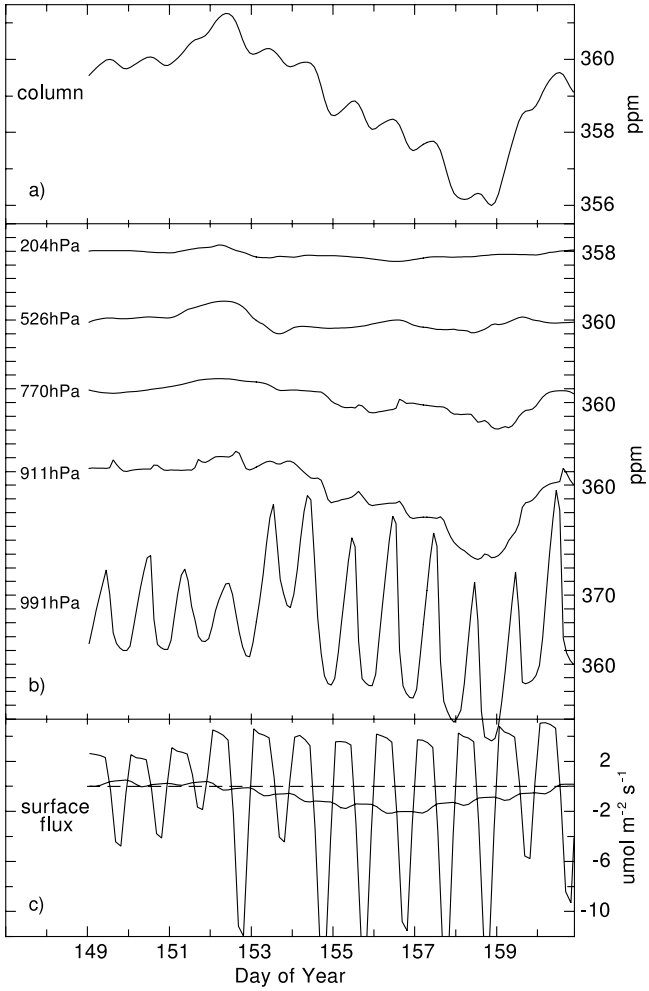

Figure 2. (a) Modeled column CO_2, (b) CO_2 mixing ratios at 991, 911, 770, 526, and 204 hPa, and (c) diurnal and 5-day running mean surface CO_2 fluxes from the model grid cell containing the Park Falls/WLEF tower site for the period from 29 May (day 149) to 10 June (day 161).

affects boundary layer mixing, photosynthesis, and ecosystem respiration [*Bakwin et al.*, 1998].

[18] MATCH model simulations with the prescribed diurnal surface fluxes as described above captured the magnitude of diurnal variability near the surface and the downward trend over this period (Figure 1a). The phase of the modeled CO_2 diurnal cycle matched the observed phase relatively well (Figure 1a, inset).

[19] Column CO_2 from the model at the same location had much smaller diurnal amplitudes, increasing from ~0.2 to 0.3 ppm in May to ~0.4 to 0.6 ppm in July (Figure 1b). In contrast to surface CO_2 where most of the variability was connected to the diurnal cycle, with column CO_2 a greater fraction of the variability was linked to events that had timescales on the order of 2 to 6 days. To influence the column, CO_2 flux anomalies had to accumulate in the lower troposphere over a period of several days or there had to be a large-scale replacement of the air within the column. A relatively large synoptic event that exhibited both these properties occurred in the model between day 150 and 160 (Figure 1b). Over this period column CO_2 rapidly decreased from day 153 through day 157 (dropping by over 5 ppm), and then reversed direction from day 158 to day 160 (increasing by over 3 ppm in less than 3 days) (Figure 2). Part of the build up of column CO_2 between day 149 and 152 can be attributed to entrainment of CO_2-enriched air from the northwest in the middle and upper troposphere at altitudes at and above 770 hPa (data not shown).

[20] The higher frequency variations caused by diurnally varying surface fluxes were progressively damped with increasing altitude. For example, at 991 hPa the diurnal components of the source are clearly visible in Figure 2 while by 911 hPa the diurnal variations are largely absent. At this level the variations more closely followed a 5-day running mean of the source. At 770 hPa the concentrations still followed the 5-day mean source but the magnitude of the variation was much smaller than at 911 hPa. At 526 hPa and above there was very little trace of any surface influence, however, horizontal mixing at this altitude (and in general in the midtroposphere) contributed to the build up of column CO_2 on day 152. This shows a distinction in the model between the planetary boundary layer which was tightly coupled to surface activity and the free troposphere which was largely decoupled from the surface on diurnal timescales.

4.2. Diurnal Column Variability in the Amazon Basin

[21] Over the Amazon site the modeled vertical CO_2 profiles were qualitatively similar to the observed profiles near the surface, but did not exhibit the same degree of variability at altitudes above 0.5 km (Figure 3). The modeled daily mean profile had a maximum near the surface from the interaction of the diurnally varying source and the height of the planetary boundary layer [*Denning et al.*, 1996a, 1999b; *Chou et al.*, 2002]. The minimum observed in the model at 0.75 km was probably caused by a "relic" boundary layer and relatively strong surface sinks in the CASA model during preceding days.

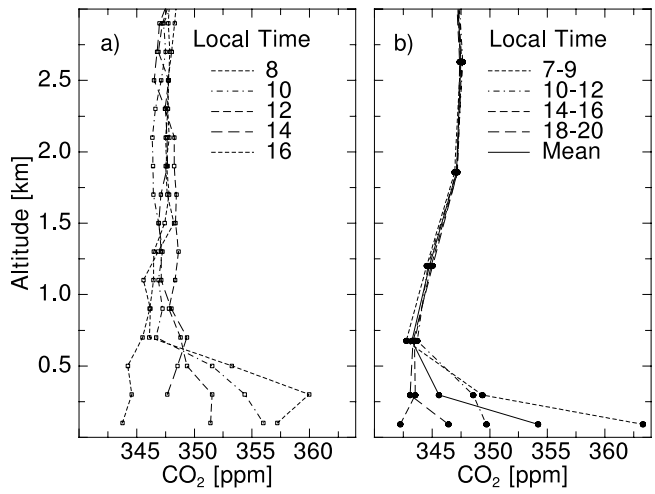

Figure 3. (a) Observed and (b) modeled CO_2 profiles in the Amazon Basin from 13 April to 5 May. The observations were made as a part of the ABLE 2B experiment in 1987 [*Fan et al.*, 1990; *Harriss et al.*, 1990] and were averaged by hour and 200 m altitude intervals. Modeled mixing ratios were adjusted so that the model mean at 3.5 km during this period was 350 ppm.

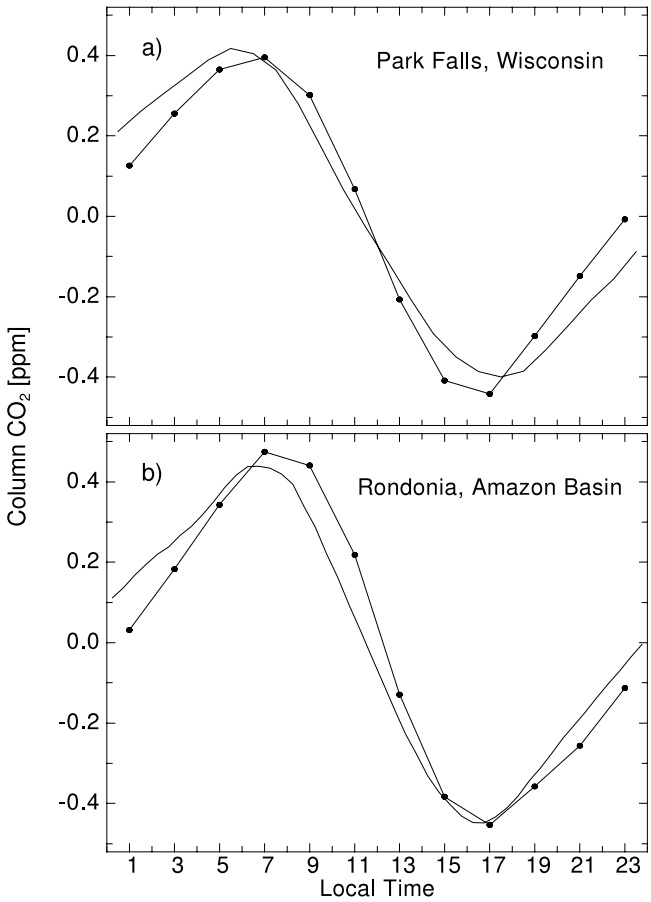

Figure 4. Column CO_2 diurnal cycles at (a) the Park Falls/WLEF tower site (46°N, 90°W) from 19 July to 17 August and (b) the Amazon Basin (10°S, 62°W) from 16 May to 15 June from the model simulation (line with dots) and calculated from the observed NEE diurnal flux assuming an isolated column (plain line). Note that in the model the 2 hour averaged data and 3 hour averaged sources introduced an uncertainty in the timing of the modeled diurnal phase of ~1 hour.

[22] Assuming no additional concentration variability above 3 km, the diurnal amplitude of the column calculated from the aircraft observations was found to be 0.92 ppm between 0800 and 1600 hours. This was approximately equal to that estimated using the eddy flux measurements of *Fan et al.* [1990] (0.98 ppm). For the same period, the column amplitude in the atmospheric model was found to be 0.60 ppm assuming no variability above 3 km and 0.62 ppm including variability above 3 km. For the same model grid cell the amplitude for an isolated column forced with the model surface fluxes would have been 0.69 ppm. The primary reason for the differences between the model and observed diurnal amplitudes was that the model surface fluxes were about 43% lower than the observations (Table 2).

4.3. Latitudinal Variability of Daytime Net Flux (DNF) and Column CO_2 Diurnal Amplitudes

[23] At the tower sites listed in Table 2, the amplitude of the column diurnal cycle in the model simulation varied between 0.41 and 0.93 ppm while the modeled surface diurnal amplitudes (in the lowest 110 m) varied between 16.5 and 32.2 ppm. Column diurnal amplitude generally increased with increasing DNF. At these sites, observed DNFs ranged from -1.7 to -6.2 gC m^{-2} d^{-1} while the modeled DNFs for the same areas and times ranged from -2.5 to -4.7 gC m^{-2} d^{-1} (Table 2). Within the Alaska and Wisconsin regions, observed DNF varied widely, as expected, from differences in vegetation type and stand age.

[24] The amplitude of the column diurnal cycle was found to be virtually negligible over northern terrestrial ecosystems during winter months and over the ocean (Table 1). At regional scales, the model predicted the largest diurnal amplitudes within the Amazon basin, with an average of 0.73 ppm in January and 0.89 ppm in July.

[25] The proportionality between DNF and column diurnal amplitudes in the model simulation was strong, but not perfect. At the tower sites (Table 2), the diurnal amplitudes from the model simulation were 10% to 32% smaller than that predicted from the modeled surface fluxes assuming an isolated column. This was probably a result of diurnal surface fluxes not reaching steady state over a 24-hour cycle, i.e., the sum of nighttime respiration fluxes were smaller in magnitude than the DNF. In this case, a portion of the DNF would have driven a decreasing trend in column CO_2 over a period of days but would not have had any direct effect on the amplitude of the column diurnal cycle. This mechanism explains why differences between model simulated diurnal amplitudes and those predicted assuming an isolated atmospheric column were greatest at northern middle and high latitudes. During summer in boreal and temperate ecosystems carbon rapidly accumulates (on the order of 1 gC m^{-2} d^{-1}) and fluxes are far from steady state [e.g., *Fung et al.*, 1983; *Randerson et al.*, 1997; *Goulden et al.*, 1997]. Much of this discrepancy can be ameliorated by linearly detrending the model sources before the DNF calculation; however some small disagreement still remains due to differences in horizontal mixing processes that entrained air over flux tower sites that had a different history of surface exchange and vertical mixing.

[26] Over highly productive terrestrial ecosystems, the diurnal cycle of modeled column CO_2 had a maximum in the early morning near sunrise and a minimum in the late afternoon, slightly before sunset; see Figure 4 for July average diurnal cycles for the Park Falls/WLEF and Rondonia tower sites. The phase of the model simulated column was largely consistent with that calculated from reported flux measurements and assuming an isolated column (Figure 4).

4.4. Seasonal Cycle of Column CO_2

[27] The amplitude of the column CO_2 seasonal cycle generally increased with latitude in the Northern Hemisphere and was much smaller than at the surface (Figure 5). At the surface, land regions in a given latitude band generally had much higher amplitudes than ocean regions. However, the column land/ocean amplitude contrast was much less pronounced than the surface. In the Northern Hemisphere, the amplitude of the column CO_2 seasonal cycle was approximately half of that predicted at the surface, both at individual NOAA/CMDL sites (Figure 6) and when the model was regionally sampled over continents and ocean basins (Table 3). Additionally, the column seasonal cycle was generally delayed in phase as compared

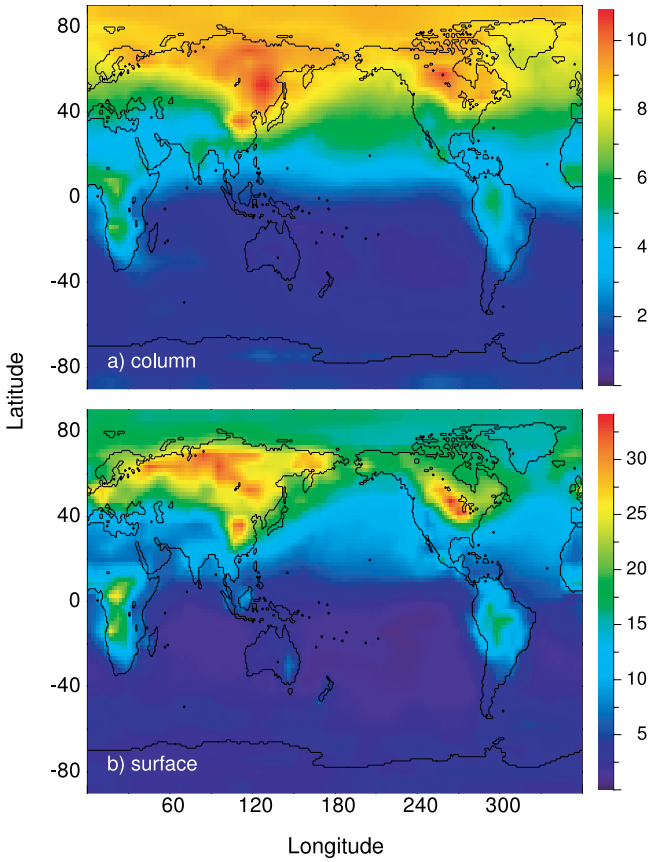

Figure 5. Modeled peak to trough seasonal amplitudes [ppm] for (a) column and (b) surface CO_2. The data were linearly detrended and smoothed with a 30 day running mean filter. Note that the two color bars have different scales.

with that at the surface, probably as a result of the time delays associated with vertical mixing and the greater mass of CO_2 in the column [e.g., *Rayner and Law*, 1995]. The magnitude of the phase delay varied by up to 7 weeks as measured by time differences associated with the timing of the minimum and maximum peaks. The lag was not always the same for the minimum and maximum points in the cycle (Table 3). At Kitt Peak, the model underestimated the observed amplitude by approximately 25% (Figure 6). It should be noted, however, that all but a few points were within standard deviation error bars of the observations.

[28] While there was evidence for a phase delay between the column and the surface in the Southern Hemisphere (e.g., the Cape Grim panel in Figure 6), the relatively small seasonal amplitudes made it difficult to separate the seasonal cycle from the long term atmospheric CO_2 growth rates caused by fossil fuel emissions.

4.5. Large-Scale Vertical and Horizontal Variability

[29] In the Northern Hemisphere midlatitudes the zonal mean CO_2 altitude profile had a large seasonal cycle whose amplitude was largest near the surface and decreased with height (Figure 7a) such that the column average CO_2 was greater than surface CO_2 in summer and fall but lower in the winter and spring. The annual mean profile decreased with height in the Northern Hemisphere primarily as a result of fossil fuel emissions at the surface and time delays associated with vertical and horizontal mixing. The "rectifier effect" interaction between biospheric emissions and seasonally varying boundary layer dynamics also contributed to high mean annual CO_2 levels near the surface and lower CO_2 levels aloft [*Denning et al.*, 1996a, 1999b]. In the Southern Hemisphere midlatitudes CO_2 profiles had the same shape throughout the year (Figure 7b). Generally the profiles increased with height from a poleward transport

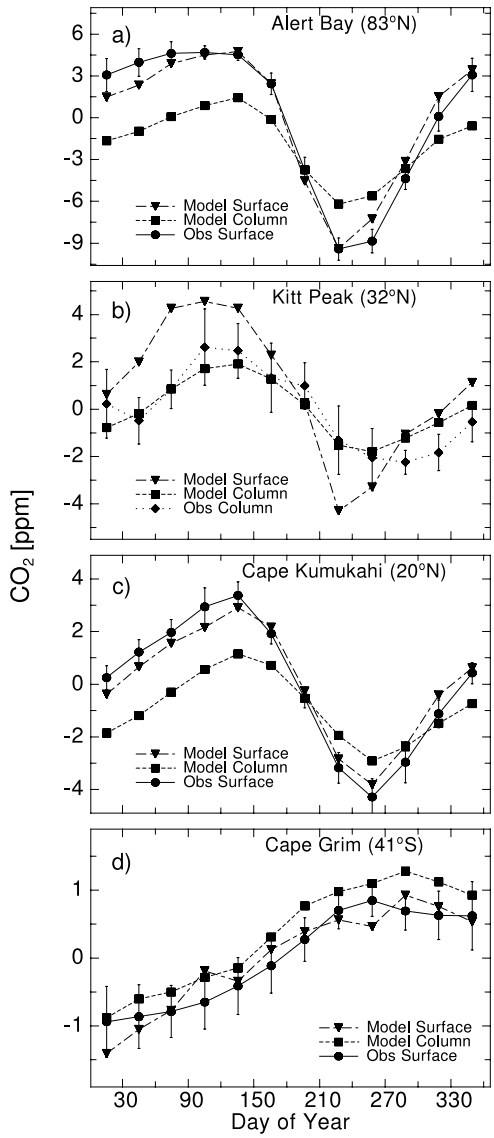

Figure 6. Modeled surface (triangles) and column (squares) CO_2 mixing ratios at (a) Alert Bay, Canada, (b) Kitt Peak, USA, (c) Cape Kumukahi, USA, and (d) Cape Grim, Australia. At Alert Bay, Cape Kumukahi, and Cape Grim, surface measurements from the NOAA/CMDL network are shown with circles and standard deviation error bars. At Kitt Peak, data from *Yang et al.* [2002] for solar zenith angles less than 80° are shown with diamonds and standard deviation error bars. To construct the model estimate of the column at Kitt Peak, we sampled the model at levels above 790 hPa, corresponding to the height of Kitt Peak (2083 m).

Table 3. Amplitude and Phase Information for the Seasonal Cycle of Surface and Column CO_2

	Seasonal Amplitude, ppm		Julian Day of Minimum Concentration[a]			Julian Day of Maximum Concentration[a]			Mean Annual Mixing Ratio[b]	
Region	Surface	Column	Surface	Column	Difference	Surface	Column	Difference	Surface	Column
Eurasia, 50°N–90°N	22.6	8.31	201	220	19	107	115	8	9.92	3.05
North America, 50°N–90°N	17.0	8.59	215	237	22	109	131	22	6.26	2.66
Eurasia, 22°N–50°N	11.5	5.06	228	236	8	107	110	3	8.32	2.76
North America, 22°N–50°N	13.4	6.06	229	239	10	105	122	17	11.18	2.85
Congo	12.0	4.50	302	305	3	14	46	32	12.74	2.67
Amazon Basin	6.6	3.44	93	140	47	48	55	6	13.65	2.37
Africa south of 0°S	9.1	3.01	80	83	3	262	263	1	6.12	1.44
Australia	1.7	0.72	—	—	—	—	—	—	2.45	0.96
South America, south of 20°S	5.4	2.10	1	9	8	249	245	−4	5.87	1.03
Pacific Ocean, 50°N–90°N	16.1	8.02	233	234	1	114	130	17	4.29	2.76
Atlantic Ocean, 50°N–90°N	15.7	7.77	227	242	16	80	124	44	4.16	2.80
Pacific Ocean, 22°N–50°N	10.8	6.03	245	250	4	125	125	0	4.74	2.79
Atlantic Ocean, 22°N–50°N	10.9	5.53	239	244	5	117	123	7	4.64	2.72
Pacific Ocean, 22°S–22°N	2.7	1.98	267	286	19	121	124	4	3.15	2.12
Atlantic Ocean, 22°S–22°N	2.7	2.29	273	289	16	79	78	−1	3.37	2.30
Pacific Ocean, 22°S–50°S	1.0	0.63	—	—	—	—	—	—	0.80	0.85
Indian Ocean, 22°S–50°S	1.7	1.22	—	—	—	—	—	—	0.35	0.68
Atlantic Ocean, 20°S–50°S	2.0	1.12	—	—	—	—	—	—	0.63	0.75
Southern Ocean, south of 50°S	2.3	1.13	—	—	—	—	—	—	−0.25	0.05

[a]The data were linearly detrended and smoothed with a 30 day running mean filter. The day of minimum and maximum are not shown where the column seasonal cycle amplitude was less than 1.5 ppm.
[b]Defined relative to the annual mean surface CO_2 in all regions south of 60°S.

of CO_2-enriched tropical air in the upper troposphere and from ocean uptake in southern midlatitudes [*Takahashi et al.*, 1999]. As a consequence, south of 30°S, column CO_2 was generally greater than surface CO_2 (Figure 8a).

[30] The north-south gradient of column CO_2 was much less variable than that predicted at the surface (Figures 8 and 9). The difference in zonal mean column CO_2 between 45°N and 45°S was approximately 2.2 ppm as compared to 7.3 ppm at the surface (Figure 8). The overall shape and sign of the gradient depended strongly on season and was greatest in spring and weakest in fall (positive defined when Northern Hemisphere mixing ratios are greater than southern). The northern midlatitude zonal monthly mean surface mixing ratio changed by ~15 ppm from February to August; the corresponding change in the column was only ~6 ppm.

[31] For the case of column CO_2, the strength of the annual north-south gradient depended only weakly on whether land or ocean regions were sampled (Table 3). For example, the mean CO_2 difference between North America (22°N to 50°N) and surface regions south of 60°S was 2.85 ppm, while the difference for the North Pacific at similar latitudes was 2.79 ppm. The land/ocean difference in the strength of the north-south column gradient differed by less than 3%. In contrast, the land/ocean difference in the north-south gradient at the surface was greater than a factor of 2 (11.2 ppm vs. 4.7 ppm). More generally, the land-ocean difference in the column north-south gradient was roughly an order of magnitude less than at the surface. This is because CO_2 is more rapidly dispersed by winds in the free troposphere than within the PBL and because there is no "rectifier effect" for column CO_2 (PBL dynamics have no direct effect on column CO_2).

[32] On seasonal timescales our model simulations provided evidence for some longitudinal variability, particularly over terrestrial regions with large photosynthetic fluxes (Figures 5 and 9). For example, the interiors of the Northern Hemisphere continents became depleted in CO_2 during

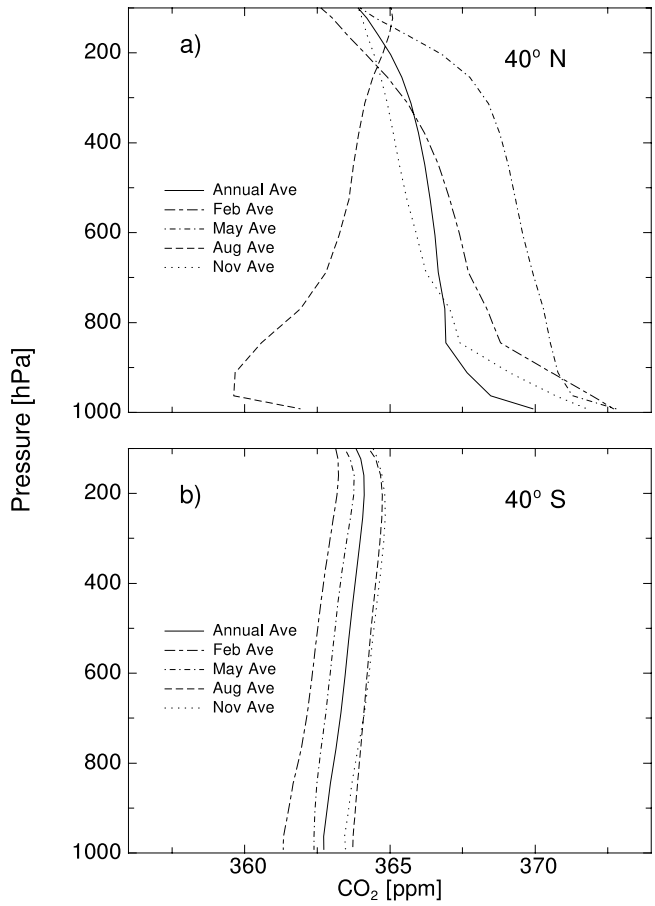

Figure 7. Modeled zonal mean CO_2 versus pressure altitude at (a) 40°N and (b) 40°S. Annual mean and February, May, August, and November monthly mean profiles are shown in each panel.

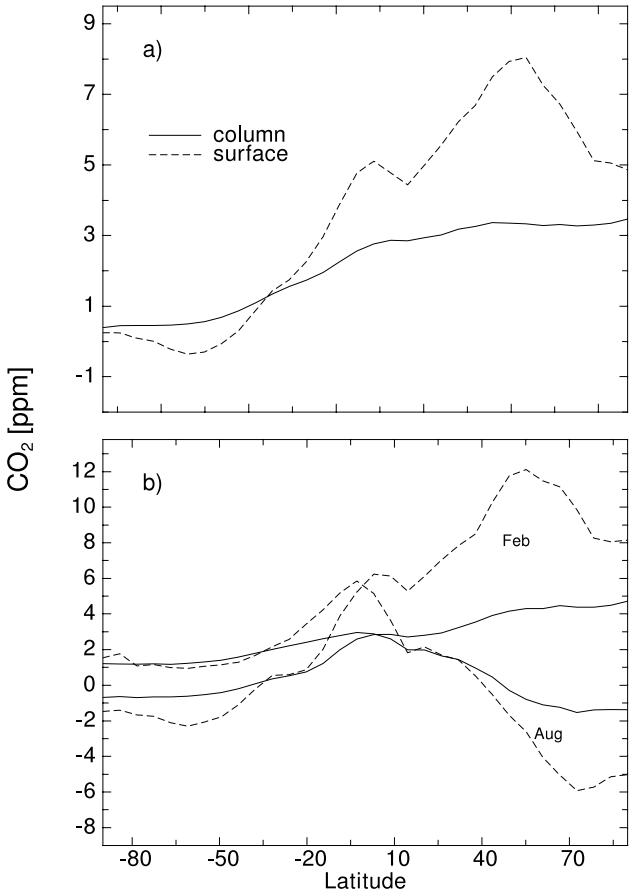

Figure 8. Modeled zonal mean surface (dashed line) and column (solid line) CO_2 as a function of latitude. (a) Annual mean north-south profiles and (b) February and August monthly means. All model values are relative to the annual mean surface mixing ratio south of 60°S such that column-surface offsets are preserved.

summer months (Figure 9). The largest longitudinal gradients occurred in the tropics, e.g., central Africa and the Amazon in February and August; however, these gradients were still much weaker than those at the surface.

5. Implications for Carbon Cycle Research

[33] While the north-south gradient of CO_2 serves as the primary evidence of the presence of a Northern Hemisphere terrestrial carbon sink, precise measurement of this gradient remains challenging because of strong vertical and horizontal gradients in CO_2 in the Northern Hemisphere (e.g., Figure 7, Table 3). Surface sampling strategies designed to minimize local contamination sources, such as minimum wind speed requirements, may also capture air masses that are more representative of the column than of the surface. For example, it can be seen from Figure 7a that if the surface were sampled under conditions that favored greater turbulent mixing, then the measured CO_2 levels would be lower, and less of a Northern Hemisphere carbon sink would be required in atmospheric inversions that did not take these effects into account. This sensitivity requires that modeling approaches sample the atmosphere in the exact same way the data were collected, e.g., under the same regime of wind speed and direction and time of day.

[34] Because there is so much less spatial variability associated with column CO_2, even with just a few observations, it will be possible to assess the strength of the Northern Hemisphere carbon sink using a measurement approach that is far less sensitive to model representations of vertical mixing. However, for the column approach to be effective, our analysis suggests that the requirements for precision and bias are strict. A 1 Gt C yr^{-1} Northern Hemisphere terrestrial carbon sink with the same distribution as fossil fuels decreased the 45°N to 45°S column CO_2 gradient by approximately 0.4 ppm in our model. Similarly, to measure the amplitude of seasonal biospheric exchange in the Northern Hemisphere to within 10% would require a precision of about 0.7 ppm, e.g., Table 3 and Figure 5. Although satellite observations may achieve comparable levels of precision from many thousands of repeated observations, they must also overcome potential biases introduced by time-varying atmospheric path lengths, surface albedo, and aerosol distributions.

[35] Column CO_2 observations of the seasonal cycle in the Northern Hemisphere in conjunction with surface observations should provide fundamental constraints on the magnitude of biospheric exchange and vertical rates of atmospheric mixing. Our current analysis provides very preliminary evidence that our CASA model estimates of growing season net flux were too weak and that the model simulated atmosphere was too vertically stratified (vertical mixing is not strong enough in the northern midlatitudes). Specifically, if we had increased our estimates of the growing season net flux, we would have no longer underestimated the seasonal amplitude of column CO_2 at the Kitt Peak Observatory; however, without simultaneously strengthening vertical mixing in the model, this would have lead to an overestimate of the surface seasonal amplitudes at Alert and Kumukahi that the model simulated reasonably well (Figure 6).

[36] In terms of future satellite design, our results suggest that sampling the atmosphere between 10 am and 2 pm would minimize any offset between the observations and the 24-hour mean (Figure 4). However, since column CO_2 is changing rapidly during this period, measurements would be highly sensitive to relatively small changes in the phase of the column cycle. Delays in satellite equator crossing times associated with a decaying orbit could potentially introduce interannual downward trends on the order of several tenths of a ppm. These trends would be greatest over highly productive terrestrial ecosystems. Regional variability in phase could also be induced by variability in the venting of nighttime CO_2 that builds up in the canopy. Assuming an isolated column, here we estimated that the phase of a column calculated from the NEE fluxes was offset from that calculated using the turbulent fluxes by over an hour. This could lead to variability over regions with dense canopies. Seasonal changes in the diurnal phase of photosynthesis linked to drought stress or cloud cover also have the potential to induce variability in column CO_2 near solar noon. Our analysis suggests that eddy covariance measurements allow for the estimation of these, and other, potential biases in column CO_2 introduced from the diurnal cycle and thus provide a means for reducing their

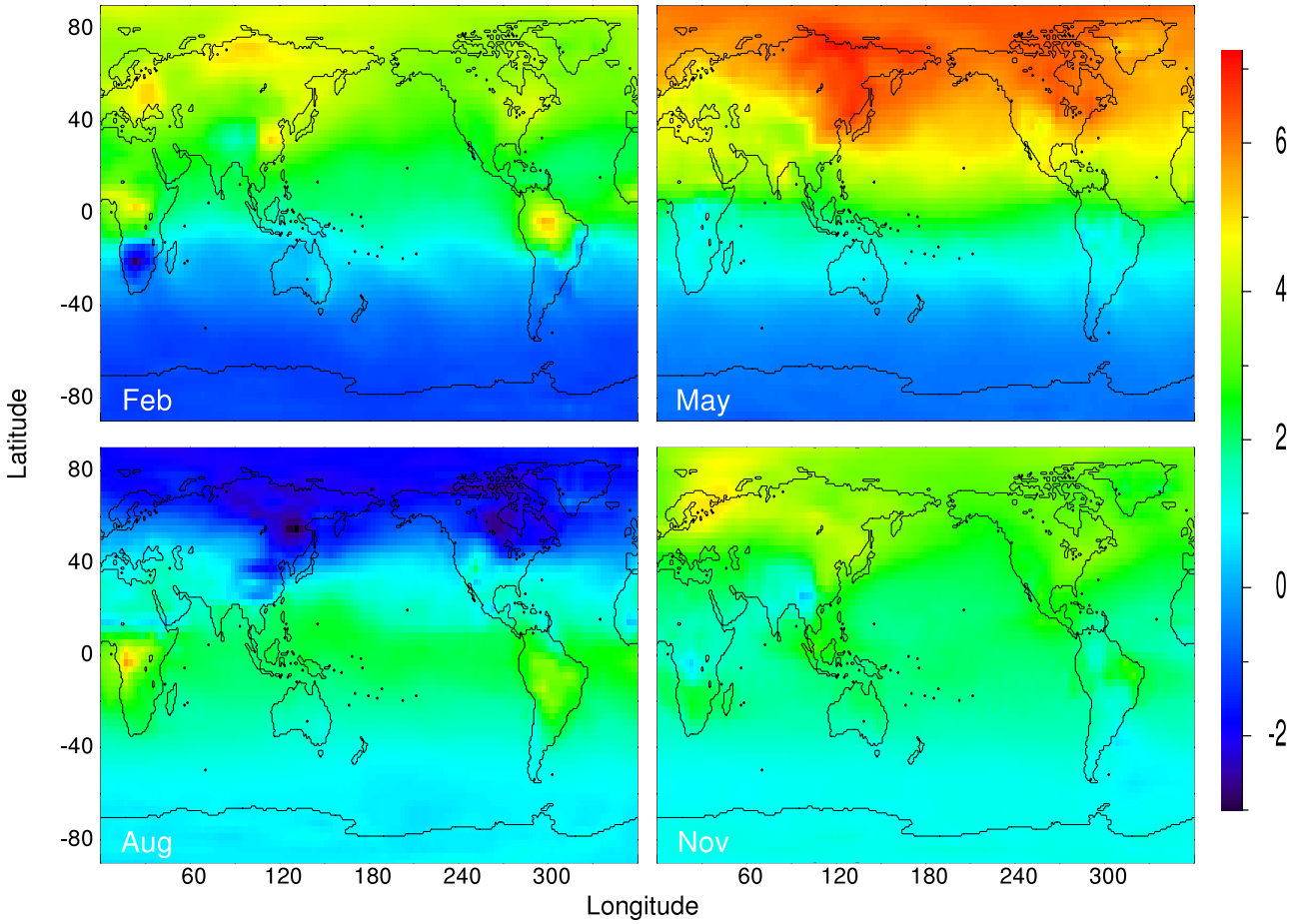

Figure 9. Modeled monthly mean column CO_2 mixing ratios [ppm] for February, May, August, and November. Values are relative to a single scalar representing the annual mean surface CO_2 mixing ratio south of 60°S.

impact on the use of column CO_2 observations in source/sink inversions.

6. Conclusions

[37] Qualitatively, column CO_2 behaves similarly to surface CO_2 but is much more uniform both spatially and temporally. The amplitude of the column CO_2 diurnal cycle is generally less than 1 ppm and its upper limit should be constrained by measurements from eddy flux towers. In the Northern Hemisphere the amplitude of the column CO_2 seasonal cycle is approximately 50% that of the surface seasonal cycle and the phase of the column is delayed relative to the surface by up to 7 weeks. With column CO_2, the longitudinal variability in the strength of the north-south gradient was found to be significantly reduced compared to surface data.

[38] **Acknowledgments.** We thank Tom Conway of NOAA/CMDL for providing CO_2 data from Cape Kumukahi, Alert Bay, and Cape Grim; Peter Bakwin of NOAA/CMDL for providing the CO_2 mixing ratio data from the Park Falls tower; and Ken Davis of Penn. State U. for providing the NEE data from the Park Falls site. This work was supported by NASA MDAR (NAG5-9462) and NSF (OPP-0097439) grants to Randerson. NCEP Reanalysis data provided by the NOAA-CIRES Climate Diagnostics Center, Boulder, Colorado, USA, from their Web site at http://www.cdc.noaa.gov. The Reserve Jaru CO_2 flux data were collected under the ABRACOS project and made available by the UK Institute of Hydrology and the Instituto Nacional de Pesquisas Espaciais (Brazil). Measurements of CO_2 fluxes (NEE) at the Park Falls tower were funded in part by the National Institute for Global Environmental Change of the U.S. Department of Energy through a grant to the University of Colorado. The carbon dioxide mixing ratio measurements, and site infrastructure and maintenance at the Park Falls tower, were supported by the Atmospheric Chemistry Project of the Climate and Global Change Program of the National Oceanic and Atmospheric Administration. We thank Zhonghua Yang for column CO_2 measurements from Kitt Peak, Heping Liu and Jamie Lindfors for eddy flux measurements from Alaska, David Noone for the CCM3 model meteorological fields, and Roger Dargaville for assistance with MATCH.

References

Andres, R. J., G. Marland, I. Fung, and E. Matthews (1996), A 1° × 1° distribution of carbon dioxide emissions from fossil fuel consumption and cement manufacture, 1950–1990, *Global Biogeochem. Cycles*, *10*, 419–429.

Bakwin, P. S., P. P. Tans, C. Zhao, W. Ussler, and E. Quesnell (1995), Measurements of carbon dioxide on a very tall tower, *Tellus, Ser. B*, *47*, 535–549.

Bakwin, P. S., P. P. Tans, D. F. Hurst, and C. Zhao (1998), Measurements of carbon dioxide on very tall towers: Results of the NOAA/CMDL program, *Tellus, Ser. B*, *50*, 401–415.

Berger, B. W., K. J. Davis, P. S. Bakwin, C. Yi, and C. Zhao (2001), Long-term carbon dioxide fluxes from a very tall tower in a northern forest: Flux measurement methodology, *J. Atmos. Oceanic Technol.*, *18*, 529–542.

Bolin, B., and C. D. Keeling (1963), Large-scale atmospheric mixing as deduced from the seasonal and meridional variations of carbon dioxide, *J. Geophys. Res.*, *68*(13), 3899–3920.

Chou, W. W., S. C. Wofsy, R. C. Harriss, J. C. Lin, C. Gerbig, and G. W. Sachse (2002), Net fluxes of CO_2 in Amazonia derived from aircraft observations, *J. Geophys. Res.*, *107*(D22), 4614, doi:10.1029/2001JD001295.

Collins, W. D., P. J. Rasch, B. E. Eaton, B. V. Khattatov, J.-F. Lamarque, and C. S. Zender (2001), Simulating aerosols using a chemical transport model with assimilation of satellite aerosol retrievals: Methodology for INDOEX, *J. Geophys. Res.*, *106*, 7313–7336.

Conway, T. J., P. P. Tans, L. S. Waterman, and K. W. Thoning (1994), Evidence for interannual variability of the carbon cycle from the National Oceanic and Atmospheric Administration Climate Monitoring and Diagnostics Laboratory global air sampling network, *J. Geophys. Res.*, *99*, 22,831–22,855.

Dargaville, R., A. D. McGuire, and P. Rayner (2002), Estimates of large-scale fluxes in high latitudes from terrestrial biosphere models and an inversion of atmospheric CO_2 measurements, *Clim. Change*, *55*, 273–285.

Dargaville, R. J., S. C. Doney, and I. Y. Fung (2003), Inter-annual variability in the interhemispheric atmospheric CO_2 gradient: Contributions from transport and the seasonal rectifier, *Tellus, Ser. B*, *55*, 711–722.

Davis, K. J., P. S. Bakwin, C. Yi, B. W. Berger, C. Zhao, R. M. Teclaw, and J. G. Isebrands (2003), The annual cycles of CO_2 and H_2O exchange over a northern mixed forest as observed from a very tall tower, *Global Change Biol.*, *9*, 1278–1293.

Denning, A. S., G. J. Collatz, C. Zhang, D. A. Randall, J. A. Berry, P. J. Sellers, G. D. Colello, and D. A. Dazlich (1996a), Simulations of terrestrial carbon metabolism and atmospheric CO_2 in a general circulation model part 1: Surface carbon fluxes, *Tellus, Ser. B*, *48*, 521–542.

Denning, A. S., D. A. Randall, G. J. Collatz, and P. J. Sellers (1996b), Simulations of terrestrial carbon metabolism and atmospheric CO_2 in a general circulation model part 2: Simulated CO_2 concentrations, *Tellus, Ser. B*, *48*, 543–567.

Denning, A. S., et al. (1999a), Three-dimensional transport and concentration of SF_6: A model intercomparison study (TransCom 2), *Tellus, Ser. B*, *51*, 266–297.

Denning, A. S., T. Takahashi, and P. Friedlingstein (1999b), Can a strong atmospheric CO_2 rectifier effect be reconciled with a "reasonable" carbon budget?, *Tellus, Ser. B*, *51*, 249–253.

Fan, S.-M., S. C. Wofsy, P. S. Bakwin, D. J. Jacob, and D. R. Fitzjarrald (1990), Atmosphere-biosphere exchange of CO_2 and O_3 in the central Amazon forest, *J. Geophys. Res.*, *95*, 16,851–16,864.

Fung, I., K. Prentice, E. Matthews, J. Lerner, and G. Russell (1983), Three-dimensional tracer model study of atmospheric CO_2: Response to seasonal exchanges with the terrestrial biosphere, *J. Geophys. Res.*, *88*, 1281–1294.

Fung, I. Y., C. J. Tucker, and K. C. Prentice (1987), Application of advanced very high-resolution radiometer vegetation index to study atmosphere-biosphere exchange of CO_2, *J. Geophys. Res.*, *92*, 2999–3015.

Gloor, M., S.-M. Fan, S. Pacala, and J. Sarmiento (2000), Optimal sampling of the atmosphere for purpose of inverse modeling: A model study, *Global Biogeochem. Cycles*, *14*, 407–428.

Goulden, M. L., B. C. Daube, S.-M. Fan, D. J. Sutton, A. Bazzaz, J. W. Munger, and S. C. Wofsy (1997), Physiological responses of a black spruce forest to weather, *J. Geophys. Res.*, *102*(D24), 28,987–28,996.

Grace, J., J. Lloyd, J. McIntyre, A. Miranda, P. Meir, H. Miranda, J. Moncrieff, J. Massheder, I. Wright, and J. Gash (1995a), Fluxes of carbon dioxide and water vapor over an undisturbed tropical forest in south-west Amazonia, *Global Change Biol.*, *1*, 1–12.

Grace, J., et al. (1995b), Carbon dioxide uptake by an undisturbed tropical rain forest in southwest Amazonia, 1992 to 1993, *Science*, *270*, 778–780.

Gurney, K. R., et al. (2002), Towards robust regional estimates of CO_2 sources and sinks using atmospheric transport models, *Nature*, *415*, 626–630.

Harriss, R. C., et al. (1990), The Amazon boundary-layer experiment: Wet season 1987, *J. Geophys. Res.*, *95*(D10), 16,721–16,736.

Hurwitz, M. D., D. M. Ricciuto, K. J. Davis, W. Wang, C. Yi, M. P. Butler, and P. S. Bakwin (2003), Advection of carbon dioxide in the presence of storm systems over a northern Wisconsin forest, *J. Atmos. Sci.*, in press.

Keeling, C. D., R. B. Bacastow, A. E. Bainbridge, C. A. Ekdahl, P. R. Guenther, L. S. Waterman, and J. F. S. Chin (1976), Atmospheric carbon dioxide variations at Mauna Loa observatory, Hawaii, *Tellus*, *28*, 538–551.

Knorr, W., and M. Heimann (1995), Impact of drought stress and other factors on seasonal land biosphere CO_2 exchange studied through an atmospheric tracer transport model, *Tellus, Ser. B*, *47*(4), 471–489.

Mahowald, N. M., P. J. Rasch, B. E. Eaton, S. Whittlestone, and R. G. Prinn (1997), Transport of ^{222}radon to the remote troposphere using the model of atmospheric transport and chemistry and assimilated winds from ECMWF and the National Center for Environmental Prediction/NCAR, *J. Geophys. Res.*, *102*, 28,139–28,151.

Masarie, K. A., and P. P. Tans (1995), Extension and integration of atmospheric carbon dioxide data into a globally consistent measurement record, *J. Geophys. Res.*, *100*(D6), 11,593–11,610.

Pak, B. C., and M. J. Prather (2001), CO_2 source inversions using satellite observations of the upper troposphere, *Geophys. Res. Lett.*, *28*, 4571–4574.

Randerson, J. T., M. V. Thompson, T. J. Conway, I. Y. Fung, and C. B. Field (1997), The contribution of terrestrial sources and sinks to trends in the seasonal cycle of atmospheric carbon dioxide, *Global Biogeochem. Cycles*, *11*, 535–560.

Rasch, P. J., X. X. Tie, B. A. Boville, and D. L. Williamson (1994), A three-dimensional transport model for the middle atmosphere, *J. Geophys. Res.*, *99*(D1), 999–1017.

Rasch, P. J., W. D. Collins, and B. E. Eaton (2001), Understanding the Indian Ocean Experiment (INDOEX) aerosol distributions with an aerosol assimilation, *J. Geophys. Res.*, *106*, 7335–7337.

Rayner, P. J., and R. M. Law (1995), A comparison of modelled responses to prescribed CO_2 sources, *Tech. Pap. 36*, Div. of Atmos. Res., Commonw. Sci. and Indust. Res. Org.

Rayner, P. J., and D. M. O'Brien (2001), The utility of remotely sensed CO_2 concentration data in surface source inversions, *Geophys. Res. Lett.*, *28*(1), 175–178.

Rayner, P. J., R. M. Law, D. M. O'Brien, T. M. Butler, and A. C. Dilley (2002), Global observations of the carbon budget, 3, Initial assessment of the impact of satellite orbit, scan geometry, and cloud on measuring CO_2 from space, *J. Geophys. Res.*, *107*(D21), 4557, doi:10.1029/2001JD000618.

Takahashi, T., R. Wanninkhof, R. Freely, R. Weiss, D. Chipman, N. Bates, J. Olafsson, C. Sabine, and S. Sutherland (1999), Net sea-air CO_2 flux over the global oceans: An improved estimate based on the sea-air pCO_2 difference, in *Proceedings of the 2nd International Symposium CO2 in the Oceans—The 12th Global Environment*, edited by Y. Nojiri, pp. 18–21, Cent. for Global Environ. Res., Natl. Inst. for Environ. Stud., Tsukuba, Japan.

Tans, P. P., I. Y. Fung, and T. Takahashi (1990), Observational constraints on the global atmospheric CO_2 budget, *Science*, *247*, 1431–1438.

Wallace, L., and W. Livingston (1990), Spectroscopic observations of atmospheric trace gases over Kitt Peak: 1. Carbon dioxide and methane from 1979 to 1985, *J. Geophys. Res.*, *95*(D7), 9823–9827.

Waugh, D. W., et al. (1997), Three-dimensional simulations of long-lived tracers using winds from MACCM2, *J. Geophys. Res.*, *102*(D17), 21,493–21,513.

Wofsy, S. C., R. C. Harriss, and W. A. Kaplan (1988), Carbon dioxide in the atmosphere over the Amazon basin, *J. Geophys. Res.*, *93*, 1377–1387.

Yang, Z., G. C. Toon, J. S. Margolis, and P. O. Wennberg (2002), Atmospheric CO_2 retrieved from ground-based near IR solar spectra, *Geophys. Res. Lett.*, *29*(9), 1339, doi:10.1029/2001GL014537.

S. C. Olsen, m/c 100-23, Division of Geological and Planetary Science, California Institute of Technology, Pasadena, CA 91125, USA. (olsen@gps.caltech.edu)

J. T. Randerson, Department of Earth System Science, University of California at Irvine, 3212 Croul Hall, Irvine, CA 92697, USA. (jranders@uci.edu)